Nuclear Engineering and Technology 55 (2023) 2166–2171

Contents lists available at ScienceDirect

Nuclear Engineering and Technology

journal homepage: www.elsevier.com/locate/net

Original Article

Experimental assessment for the photon shielding features of silicone rubber reinforced by tellurium borate oxides

M. Elsafi [a, *], Heba jamal ALasali [b], Aljawhara H. Almuqrin [c], K.G. Mahmoud [d], M.I. Sayyed [b, e]

[a] Physics Department, Faculty of Science, Alexandria University, 21511, Alexandria, Egypt
[b] Department of Physics, Faculty of Science, Isra University, Amman, Jordan
[c] Department of Physics, College of Science, Princess Nourah Bint Abdulrahman University, P.O. Box 84428, Riyadh, 11671, Saudi Arabia
[d] Ural Federal University, Mira St, 19, 62002, Yekaterinburg, Russia
[e] Department of Nuclear Medicine Research, Institute for Research and Medical Consultations (IRMC), Imam Abdulrahman Bin Faisal University (IAU), P.O. Box 1982, Dammam, 31441, Saudi Arabia

ARTICLE INFO

Article history:
Received 16 November 2022
Received in revised form
5 February 2023
Accepted 14 February 2023
Available online 24 February 2023

Keywords:
Silicone rubber
Tellurium oxide
Borate oxide
Hyper pure germanium

ABSTRACT

In the present study, six silicone rubber doped by tellurium borate oxides were fabricated using the casting method. The densities of the fabricated silicon rubber-doped by tellurium borate oxides samples were measured using the Archimedes Method. Moreover, the linear attenuation coefficient of silicone rubber doped tellurium borate oxides samples was evaluated experimentally using the hyper pure germanium, and the recorded linear attenuation coefficient values were affirmed using the theoretical Phy-X program. The experimental measurements were performed using the narrow beam transmission method with radioactive isotopes Am-241, Cs-137, and Co-60 with energies of 59, 661, 1173, and 1332 keV. The linear attenuation coefficient values showed an enhancement by 4.73 times, 1.20 time, 1.17, time, and 1.17 time, respectively at gamma photon energies of 59, 661, 1173, and 1332 keV, when the TeO_2 concentration increased in the fabricated composites from 0 to 50 wt%. The enhancement of the linear attenuation coefficient values has a positive effect on the transmission rate values where the half-value thickness and transmission rate were decreased accompanied by an increase in the RPE.

1. Introduction

As a result of its high penetrability and potentially harmful impacts on the human body, gamma ray poses a significant threat to the safety of employees in the nuclear power industry and in radiation treatment; consequently, radiation safety design in radioactive equipment has emerged as an important concern in recent years. New progress in movable nuclear plants and facilities for the disposal of nuclear waste has resulted in new prerequisites for integrated designs that are light, functional, and provide radiation shielding. On the other hand, traditional radiation shielding components like cementitious materials, iron, and lead are either heavy, hazardous or have poor mechanical properties, making it difficult for them to reach the stringent requirements of new radiation shielding configuration [1–10]. There has been a lot of research conducted on polymer matrix composites that are employed as radiation protection components [11–14]. Polymeric composite materials have the potential for possible utilization in the radiation shielding industry due to their low density, ease of processing, multifunctional property, and tailorable shielding competence.

Silicone rubber is known for its high levels of elasticity and low production costs. As a result of its durability, ease of manufacture, and ability to take on a number of different forms, silicon rubber is used in an extremely diverse range of applications [15,16]. Previous research has examined the possibility of using radiation shielding applications for these rubbers by adding PbO as well as other filler components [17–19].

Additives, such as TeO_2, Sb_2O_3, WO_3, and Bi_2O_3 may be included in the polymers of the rubbers in order to enhance the materials' capacity to shield the ionization radiation. These additions raise the likelihood that the shield will have some sort of interaction with the photons that are entering the system, hence increasing the amount of radiation that is absorbed [20–22].

* Corresponding author.
E-mail address: mohamedelsafi68@gmail.com (M. Elsafi).

https://doi.org/10.1016/j.net.2023.02.022

Simulation based on the Monte Carlo method is utilized extensively in radiation protection. A precise evaluation of the radiation shielding parameters, including the attenuation factors that may be used to determine the performance of the shielding materials, can be achieved with the assistance of this technique (i.e Monte Carlo simulation) [23–26].

In this work, Silicone rubber composites embedded with TeO_2 and B_2O_3 were used as shielding flexible materials against ionizing radiation, where the attenuation coefficients were calculated at different energies of incident photons by experimental measurements and confirmed by theoretical techniques.

2. Materials and methods

In the present work, silicone rubber with its hardener was used as a matrix mixture while tellurium dioxide (TeO_2) and boron oxide (B_2O_3) were utilized as fillers. The used silicone rubber has the same properties as the previous works [27–29], the average size of filler oxides was 50 ± 10 μm. The silicone rubber composites are manufactured according to the weight ratio shown in Table 1, where the mixture was stirred for 10 min to obtain a homogeneous mixture and then poured into molds and left for 24 h to solidify and become flexible.

The flexible samples were experimentally exposed to gamma photons from different sources (therefore, different energies include low (Am-241, 59 keV), medium (Cs-137, 662 keV), and high (Co-60, 1173 and 1333 keV) energies. These photons were detected by high resolution (1.92 keV at 1333 keV) and efficient (24%) HPGe detector. The count rate was calculated due to the photon's interactions with the detector crystal in case the presence and the absence of a flexible SR-PT sample, where the SR-PT sample was placed axially between the source and the detector, as shown in Fig. 1. The distance between the detector-to-source and the sample was chosen as previously calibrated using materials with known attenuation coefficient such as copper and aluminum. From the count rate calculation, the LAC can be calculated by the next formula [30–32]:

$$\mu = -\frac{1}{x} ln\frac{C}{C_0} \quad (1)$$

where the C_t and C_0 are the count rates recorded by the detector in the absence and presence of the fabricated SR-BT samples. The experimental linear attenuation coefficient (μ, cm^{-1}) results were compared with the values obtained from Phy-X [33]. The half-value thickness ($\Delta_{0.5}$) and mean free path (λ) are the shielding parameters that describe the attenuation efficiency of the shielding material depending on the experimentally measured μ values, as illustrated below in equations (2) and (3) [34–36]:

Table 1
The weight percentage of the fabricated silicone rubber mixture.

Composite code	Weight percentages (%)			Density, g/cm^3
	Silicone rubber	TeO_2	B_2O_3	
SR-BT0	40	–	60	1.770
SR-BT10	40	10	50	1.845
SR-BT20	40	20	40	1.928
SR-BT30	40	30	30	2.018
SR-PT40	40	40	20	2.118
SR-PT50	40	50	10	2.227

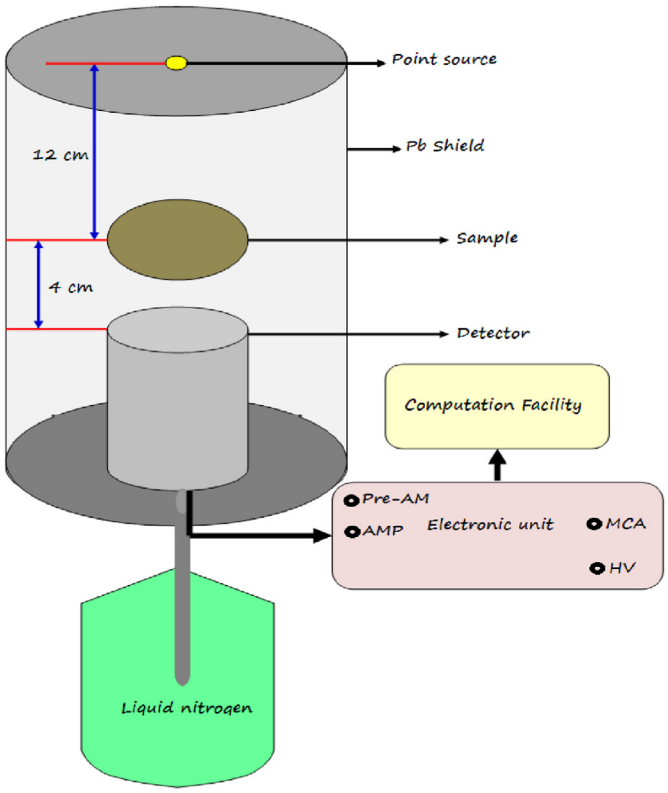

Fig. 1. The geometry of the experimental work.

$$\Delta_{0.5} = \frac{\ln 2}{\mu} \quad (2)$$

$$\lambda = \frac{1}{\mu} \quad (3)$$

3. Results and discussion

The LAC (or μ) was measured experimentally for the prepared SR-BT composites using the narrow bean transmission method. The measurements were performed using three different γ-ray energies Am-241, Cs-137, and Co-60, that emit photon energies of 59, 661, 1173, and 1332 keV. The experimental μ values for the fabricated Sr-BT composite were compared to the μ values calculated theoretically using the Phy-XPSD free program. The difference (δ, %) between the experimental and Phy-X/PSD results is ranged between ±1, as illustrated in Fig. 2. Fig. 2 also describes modes of variation of the μ results for the SR-BT composites versus the incident γ-photons. The first observation is the high values of μ values at E_γ of 59 keV compared with the μ results at various studied E_γ. The μ for the Sr-BT composites are 0.368, 1.418, 2.561, 5.801, 5.187, and 6.702 cm^{-1} for SR-BT0, SR-BT10, SR-BT20, SR-BT30, SR-BT40, and SR-BT50, respectively. These values are considered the highest compared to the selected various E_γ in the current study. The E_γ value of 59 keV (Am- 241) lies in the interval of photoelectric interaction in which the cross-section varied reversely with $E^{3.5}$ [37,38]. Thus, as the smallest incoming photon E_γ, the highest cross-section of interaction is associated with high values of the μ values. After that, for the isotopes Cs-137 and Co-60, the μ values minimized linearly with raising the E_γ photons. The μ values were

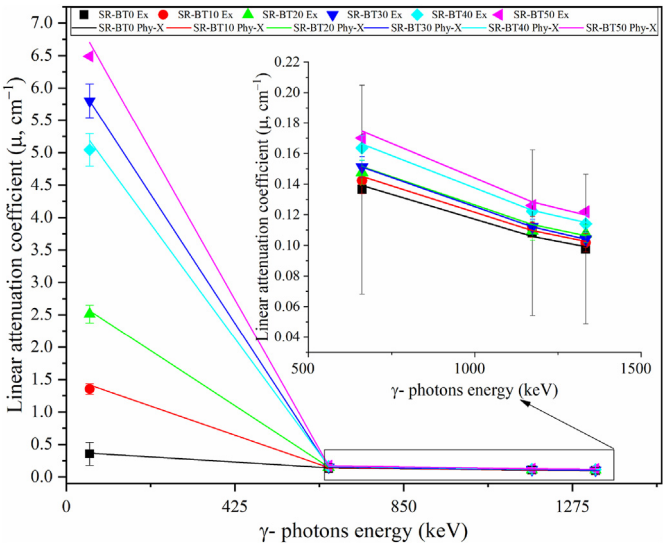

Fig. 2. The linear attenuation coefficient versus the incoming γ-ray photons.

minimized by 28.7%, 29.2%, 29.8%, 31.1%, 30.8%, and 31.3% for samples SR-BT0, SR-BT10, SR-BT20, SR-BT30, SR-BT40, and SR-BT50, respectively, when the E_γ values raised from 662 to 1332 keV. This behavior is related to the Compton Scattering. The cross-section in the mentioned interval is inversely varied with E. Thus, the cross-section diminished linearly with raising the E_γ values, which causes a linear decrease in the μ.

Fig. 3 describes the incrementation of the TeO_2 effects on the fabricated SR-BT composites μ values. The obtained experimental results refer that the replacement of B_2O_3 concentration by TeO_2 compound in the fabricated SR-BT composites has a great effect on the low E_γ values (i.e., 59 keV), but this effect is diminished with raising the E_γ values (i.e., 662 keV, and 1252 keV). At 59 keV, the enhancement in the μ values for SR-BT50 (50 wt.% of TeO_2) composite reaches 4.73 times higher than the SR-BT0 (0 wt.% of TeO_2). This high percentage of enhancement is attributed to the photoelectric interaction cross-section and effective atomic number (Z_{eff}), since the cross-section is directly changed with Z_{eff}^{4-5} [39,40].

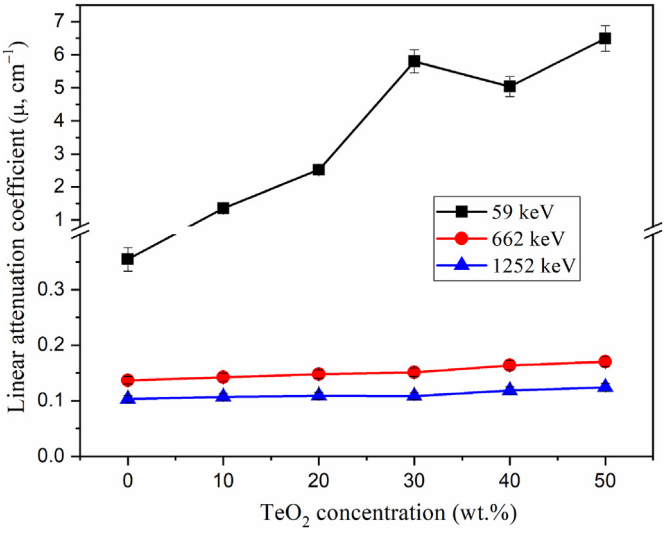

Fig. 3. Dependence of the LAC on the TeO_2 concentration of the fabricated SR-BT composites.

The replacement of the B_2O_3 compound with the TeO_2 compound causes a significant increase in the density of the given composites which leads to an increase in the effective atomic number of the fabricated composites. Thus, the interaction cross-section is notably increased. The net results are a high increase in the energy consumed by photons to escape from the composite thickness, associated with an increase in the μ for the composites. In contrast for intermediate E_γ values, the enhancement on the μ is very small compared to that achieved at E_γ of 59 keV where the μ values were enhanced by factors of 25% and 20% for E_γ of 662 and 1252 keV, respectively. This behavior is related to the CS cross-section which is proportional to Z. So, a linear increase in the interaction cross-section is associated with an increase in the Z_{eff} of the fabricated composite.

The $\Delta_{0.5}$ refers to the fabricated SR-BT composites' thickness ability to minimize the intensity of the utilized γ-photon sources by 50%. The $\Delta_{0.5}$ was calculated based on the experimental μ data. Fig. 4 depicts a high increase in the $\Delta_{0.5}$ at the low E_γ interval followed by a linear increase in the intermediate energy region between (662 keV < E_γ<1332 keV). The previous trends are attributed to the interaction mode (photoelectric or Compton scattering), where the cross-section of interaction varied inversely with $E^{3.5}$ and E for photoelectric and Compton interaction, respectively, as early illustrated in the discussion of μ section. The decrease in the cross-section with raising the E_γ values leads to a significant decrease in the μ values of the fabricated SR-BT composites. Thus, a lot of incident photons can ease penetrate the composite thickness, therefore, a thicker layer of the fabricated composites is required for stopping half of the incident γ-photons. The $\Delta_{0.5}$ values were grow by 3.6 times, 13.3 times, 23.3 times, 55.7 times, 44.2 times, and 53.2 times for samples SR-BT0, SR-BT10, SR-BT20, SR-BT30, SR-BT40, and SR-BT50, respectively when the γ-photon energy ranged between 59 keV and 1332 keV.

The relation length (λ, cm) is the distance inside the shield in which the photon moves between two followed collisions with the surrounding electrons. It has the same variation mode with Eγ as that early discussed in the $\Delta_{0.5}$ section. The impact of TeO_2 addition on the values of $\Delta_{0.5}$ and λ which were calculated based on the experimental μ values was clarified in Fig. 5 at two fixed energies (59 keV and 1252 keV). The figure reveals that increasing the incrementation ratio of TeO_2 causes a decrease in both $\Delta_{0.5}$ and λ. At 59 keV, the $\Delta_{0.5}$ changed from 0.51 to 0.11 cm, and the λ varied between 2.82 and 0.15 cm, respectively. Besides, for E_γ of 1252 keV,

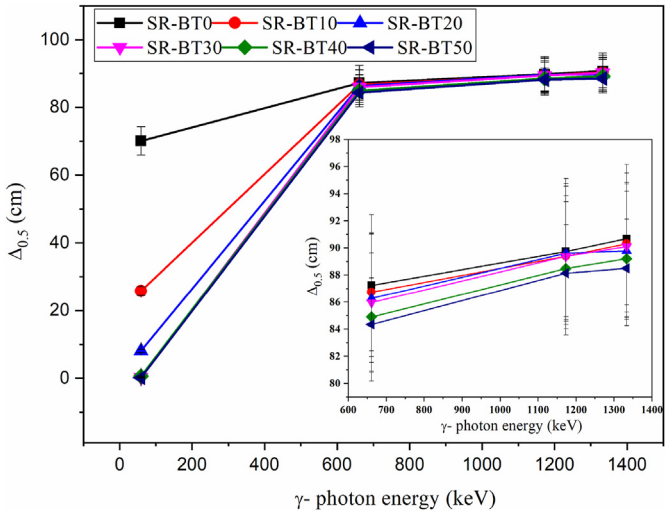

Fig. 4. The half value thickness for the current composites.

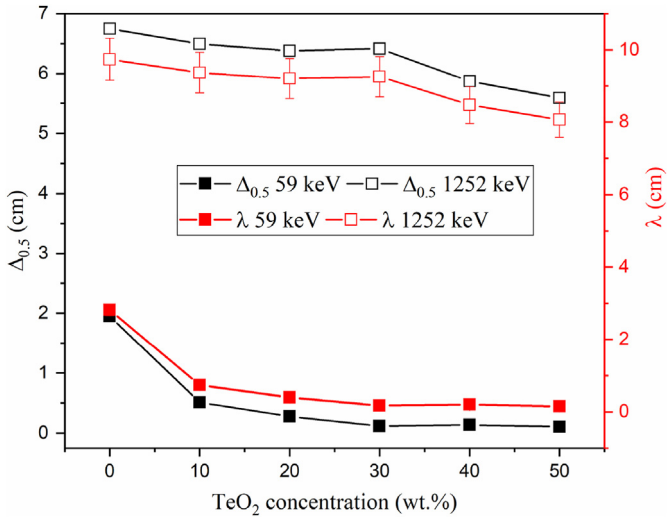

Fig. 5. Impact of the TeO_2 incrementation ratio on both half values thickness, and relaxation length (λ).

the $\Delta_{0.5}$ decreased from 6.75 to 5.59 cm and the λ diminished from 9.74 to 8.06 cm, respectively. Such change in both $\Delta_{0.5}$ and λ is ascribed to the increase in the composite density due to the substitution of B_2O_3 by TeO_2 compounds. The mentioned substitution increases the ability of the fabricated composite to resist the incoming photons. As a result, the net number of photons penetrating the shield thickness decreased as increased the substitution ratio.

The TF is the number of photons that escape from the composite (C_t) to the initial total number of γ-photons (C_o). Further, the number of γ-photons that couldn't escape and annihilated inside the composite (C_a) to the total initial number of γ-photons (C_o) is called RPE. The TF and RPE are influenced by many factors such as E_γ, the substitution of the B_2O_3 by TeO_2, and the thickness of the given composites.

The impacts of the incoming E_γ on the TF and RPE for the investigated composites were discussed in Fig. 6. The data depicts an increase in the TF (for both SR-BT 0 and SR-BT40) accompanied by an equal reduction in the RPE (for both SR-BT 0 and SR-BT40) when the E_γ raised from 59 to 1332 keV. For example, the fabricated composite SR-BT0 has TF values from 70.12% to 90.70%, but the RPE diminished from 29.88% to 9.30%, between 59 and 1332 keV, respectively. Also, for the fabricated composite SR-BT40, the TF raised from 0.15% to 88%, but the RPE was reduced by a factor of 88% by raising the E_γ in the same energy interval. The previously mentioned behaviors can be explained based on the penetration power of γ-photons that increased with raising the E_γ. Accordingly, C_t photons increased accompanied by an equivalent decrease in the C_a photons.

The influence of the partial substitution of B_2O_3 by TeO_2 on the TF and RPE was also discussed in Fig. 7, for some fixed E_γ values (59 and 1252 keV). The substitution of B_2O_3 by TeO_2 causes an increase in the molecular mass, Z_{eff}, and density of the selected composites where the incrementation of TeO_2 by ratios varied between 0 and 40 wt%, causes an increase in the composites' ρ values from 1.770 to 2.227 g/cm^3. The illustrated increase in the composites' ρ leads to an increase in the μ of the fabricated composites. This is associated with an increase in the C_a photon number and a decrease in the C_t photon numbers. The net result is an increase in the RPE values. At 59 keV, a thickness of 1 cm of the fabricated composites was able to increase the RPE from 74.20% to 99.85% while the TF values reduced from 70.12% to 0.15% when the TeO_2 increased from 0 wt% to 40 wt% respectively.

The fabricated composite thickness also plays an important role in controlling the TF and RPE values (Fig. 8). The results of these factors against the composite thickness depict a high increase in the RPE accompanied by an equal decrease in the TF by raising the thickness between 0.5 and 5 cm. At 59 keV, the fabricated composite SR-BT 40 has the ability to enhance slightly the RPE values from 9.30% to 11.48% while the TF values for the same composite reduced from 90.70% to 88.52%, raising the thickness from 0.5 cm to 5 cm, respectively. The increase in the composite thickness higher than the λ values of the composite helps the emitted γ-photons to make more interactions along its pass length inside the composite. Therefore, the amount of E_γ consumed in the composite layer increases associated with an increase in the I_a and a decrease in the C_t photon numbers.

4. Conclusion

Six silicon rubber samples reinforced with a mixture of B_2O_3 and TeO_2 were fabricated using the casting method. The density of the

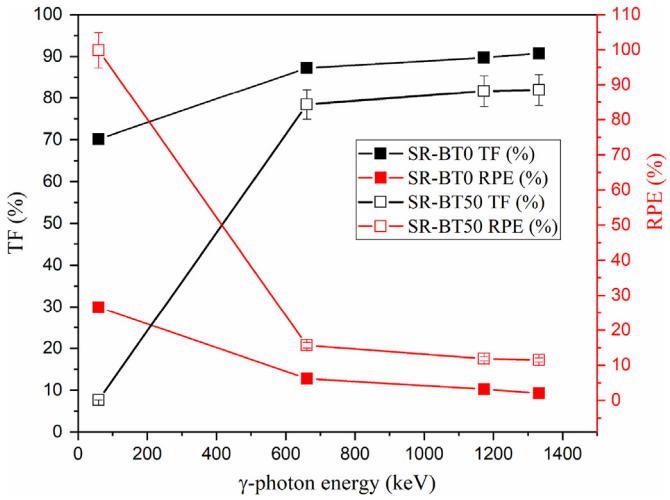

Fig. 6. Impacts of the energy on the values of transmission value (TF) and RPE.

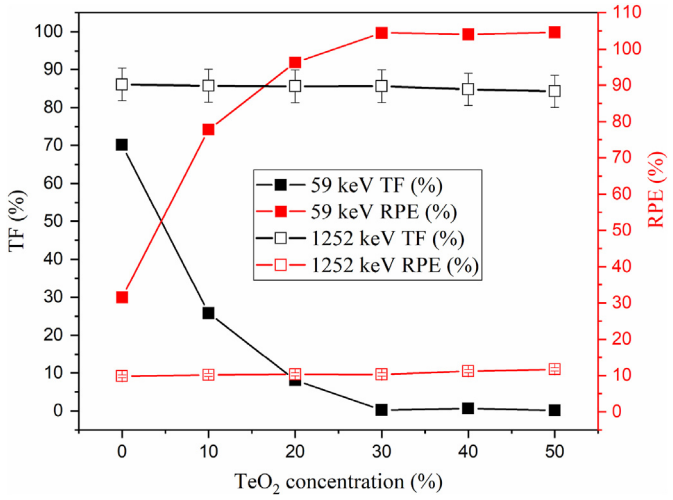

Fig. 7. Impacts of the TeO_2 incrementation on the transmission value and radiation protection efficiency.

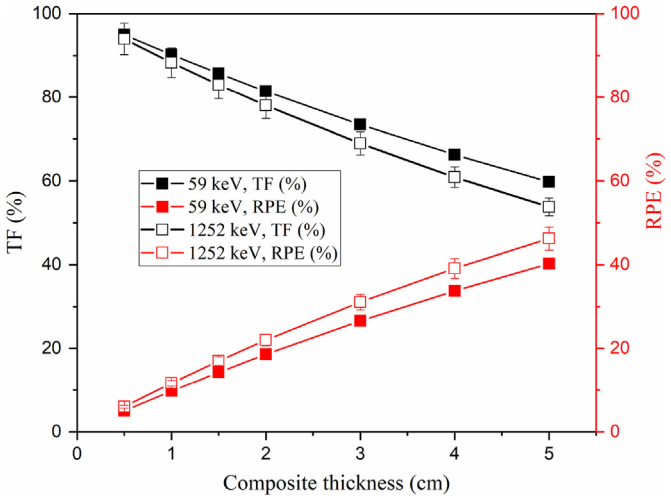

Fig. 8. Influence of the fabricated composite thickness on the values of transmission value (TF) and RPE for the SR-BT40 sample.

current samples changed between 1.770 and 2.227 g/cm^3 with increasing the TeO_2 content between 0 and 50 wt%. The experimental measurements used the hyper pure germanium to evaluate the LAC of the fabricated composites between 59 and 1.25 MeV. The measurements illustrated that the LAC increased from 0.368 to 6.702 cm^{-1} at a gamma photon energy of 59 keV, when the TeO_2 concentration increased between 0 and 40 wt%, respectively. Moreover, at the same energy, the $\Delta_{0.5}$ values also reduced by a factor of 94%, and the TF values decreased from 75% to 0.15%.

Declaration of competing interest

The authors declare that they have no known competing financial interests or personal relationships that could have appeared to influence the work reported in this paper.

Acknowledgment

The authors express their gratitude to the Princess Nourah bint Abdulrahman University Researchers Supporting Project number (PNURSP2023R2), Princess Nourah bint Abdulrahman University, Riyadh, Saudi Arabia.

References

[1] B. Aygün, High alloyed new stainless steel shielding material for gamma and fast neutron radiation, Nucl. Eng. Technol. 52 (2020) 647–653, https://doi.org/10.1016/j.net.2019.08.017.
[2] B. Aygün, Neutron and gamma radiation shielding Ni based new type super alloys development and production by Monte Carlo Simulation technique, Radiat. Phys. Chem. 188 (2021), 109630, https://doi.org/10.1016/j.radphyschem.2021.109630.
[3] M. Kamislioglu, An investigation into gamma radiation shielding parameters of the (Al:Si) and (Al+Na):Si-doped international simple glasses (ISG) used in nuclear waste management, deploying Phy-X/PSD and SRIM software, J. Mater. Sci. Mater. Electron. 32 (2021) 12690–12704, https://doi.org/10.1007/s10854-021-05904-8.
[4] M. Kamislioglu, Research on the effects of bismuth borate glass system on nuclear radiation shielding parameters, Results Phys. 22 (2021), 103844, https://doi.org/10.1016/j.rinp.2021.103844.
[5] K.A. Naseer, G. Sathiyapriya, K. Marimuthu, T. Piotrowski, M.S. Alqahtani, E.S. Yousef, Optical, elastic, and neutron shielding studies of Nb2O5 varied Dy3+ doped barium-borate glasses, Optik 251 (2022), 168436, https://doi.org/10.1016/j.ijleo.2021.168436.
[6] Y. Al-Hadeethi, M.I. Sayyed, Radiation attenuation properties of Bi2O3–Na2O– V2O5– TiO2–TeO2 glass system using Phy-X/PSD software, Ceram. Int. 46 (2020) 4795–4800, https://doi.org/10.1016/j.ceramint.2019.10.212.
[7] A. Kumar, S.P. Singh, Y. Elmahroug, U. Kara, H.O. Tekin, M.I. Sayyed, Gamma ray shielding studies on 26.66 B_2O_3 –16GeO_2 –4Bi_2O_3 –(53.33–x) PbO–xPbF_2 glass system using MCNPX, Geant4 and XCOM, Mater. Res. Express 5 (2018), 095203, https://doi.org/10.1088/2053-1591/aad821.
[8] G. Lakshminarayana, A. Kumar, H.O. Tekin, S.A.M. Issa, M.S. Al-Buriahi, M.G. Dong, D.-E. Lee, J. Yoon, T. Park, Probing of nuclear radiation attenuation and mechanical features for lithium bismuth borate glasses with improving Bi2O3 content for B2O3 + Li2O amounts, Results Phys. 25 (2021), 104246, https://doi.org/10.1016/j.rinp.2021.104246.
[9] D.A. Aloraini, A.H. Almuqrin, M.I. Sayyed, H. Al-Ghamdi, A. Kumar, M. Elsafi, Experimental investigation of radiation shielding competence of Bi2O3-CaO-K2O-Na2O-P2O5 glass systems, Materials 14 (2021) 5061, https://doi.org/10.3390/ma14175061.
[10] G. Lakshminarayana, Y. Elmahroug, A. Kumar, M.G. Dong, D.-E. Lee, J. Yoon, T. Park, TeO2–B2O3–ZnO–La2O3 glasses: γ-ray and neutron attenuation characteristics analysis by WinXCOM program, MCNP5, Geant4, and Penelope simulation codes, Ceram. Int. 46 (2020) 16620–16635, https://doi.org/10.1016/j.ceramint.2020.03.235.
[11] T. Korkut, Z.I. Umaç, B. Aygün, A. Karabulut, S. Yapıcı, R. Şahin, Neutron equivalent dose rate measurements of gypsum-waste tire rubber layered structures, Int. J. Polym. Anal. Char. 18 (2013) 423–429, https://doi.org/10.1080/1023666X.2013.814025.
[12] N. Şahin, M. Bozkurt, Y. Karabul, M. Kılıç, Z.G. Özdemir, Low cost radiation shielding material for low energy radiation applications: epoxy/Yahyali Stone composites, Prog. Nucl. Energy 135 (2021), 103703, https://doi.org/10.1016/j.pnucene.2021.103703.
[13] S.H. Hosseini, Study on hard X-ray absorbing properties of nanocluster polyaniline, Mater. Sci. Semicond. Process. 39 (2015) 90–95, https://doi.org/10.1016/j.mssp.2015.04.050.
[14] R. Li, Y. Gu, G. Zhang, Z. Yang, M. Li, Z. Zhang, Radiation shielding property of structural polymer composite: continuous basalt fiber reinforced epoxy matrix composite containing erbium oxide, Compos. Sci. Technol. 143 (2017) 67–74, https://doi.org/10.1016/j.compscitech.2017.03.002.
[15] T. Özdemir, S.N. Yılmaz, Mixed radiation shielding via 3-layered polydimethylsiloxane rubber composite containing hexagonal boron nitride, boron (III) oxide, bismuth (III) oxide for each layer, Radiat. Phys. Chem. 152 (2018) 17–22, https://doi.org/10.1016/j.radphyschem.2018.07.007.
[16] R. Prasad, A.R. Pai, S.O. Oyadiji, S. Thomas, S.K.S. Parashar, Utilization of hazardous red mud in silicone rubber/MWCNT nanocomposites for high performance electromagnetic interference shielding, J. Clean. Prod. 377 (2022), 134290, https://doi.org/10.1016/j.jclepro.2022.134290.
[17] N. Nagaraj, H.C. Manjunatha, Y.S. Vidya, L. Seenappa, K.N. Sridhar, P.S. Damodara Gupta, Investigations on Lanthanide polymers for radiation shielding purpose, Radiat. Phys. Chem. 199 (2022), 110310, https://doi.org/10.1016/j.radphyschem.2022.110310.
[18] M. Almurayshid, S. Alsagabi, Y. Alssalim, Z. Alotaibi, R. Almsalam, Feasibility of polymer-based composite materials as radiation shield, Radiat. Phys. Chem. 183 (2021), 109425, https://doi.org/10.1016/j.radphyschem.2021.109425.
[19] N. Ekinci, K.A. Mahmoud, S. Sarıtaş, B. Aygün, M.M. Hessien, I. Bilici, Y.S. Rammah, Development of Tincal based polypropylene polymeric materials for radiation shielding applications: experimental, theoretical, and Monte Carlo investigations, Mater. Sci. Semicond. Process. 146 (2022), 106696, https://doi.org/10.1016/j.mssp.2022.106696.
[20] M.R. Ambika, N. Nagaiah, V. Harish, N.K. Lokanath, M.A. Sridhar, N.M. Renukappa, S.K. Suman, Preparation and characterisation of Isophthalic-Bi2O3 polymer composite gamma radiation shields, Radiat. Phys. Chem. 130 (2017) 351–358, https://doi.org/10.1016/j.radphyschem.2016.09.022.
[21] S. Kim, Y. Ahn, S.H. Song, D. Lee, Tungsten nanoparticle anchoring on boron nitride nanosheet-based polymer nanocomposites for complex radiation shielding, Compos. Sci. Technol. 221 (2022), 109353, https://doi.org/10.1016/j.compscitech.2022.109353.
[22] T. Özdemir, A. Güngör, I.K. Akbay, H. Uzun, Y. Babucçuoglu, Nano lead oxide and epdm composite for development of polymer based radiation shielding material: gamma irradiation and attenuation tests, Radiat. Phys. Chem. 144 (2018) 248–255, https://doi.org/10.1016/j.radphyschem.2017.08.021.
[23] A.S. Abouhaswa, M.I. Sayyed, K.A. Mahmoud, Y. Al-Hadeethi, Direct influence of mercury oxide on structural, optical and radiation shielding properties of a new borate glass system, Ceram. Int. 46 (2020) 17978–17986, https://doi.org/10.1016/j.ceramint.2020.04.112.
[24] Y.S. Rammah, I.O. Olarinoye, F.I. El-Agawany, K.A. Mahmoud, I. Akkurt, E. Yousef, Evaluation of radiation shielding capacity of vanadium–tellurite–antimonite semiconducting glasses, Opt. Mater. 114 (2021), 110897, https://doi.org/10.1016/j.optmat.2021.110897.
[25] K.A. Naseer, K. Marimuthu, K.A. Mahmoud, M.I. Sayyed, The concentration impact of Yb3+ on the bismuth boro-phosphate glasses: physical, structural, optical, elastic, and radiation-shielding properties, Radiat. Phys. Chem. 188 (2021), 109617, https://doi.org/10.1016/j.radphyschem.2021.109617.
[26] R.A.R. Bantan, M.I. Sayyed, K.A. Mahmoud, Y. Al-Hadeethi, Application of experimental measurements, Monte Carlo simulation and theoretical calculation to estimate the gamma ray shielding capacity of various natural rocks, Prog. Nucl. Energy 126 (2020), 103405, https://doi.org/10.1016/j.pnucene.2020.103405.
[27] H. Al-Ghamdi, H.M. Hemily, I.H. Saleh, Z.F. Ghataas, A.A. Abdel-Halim, M.I. Sayyed, S. Yasmin, A.H. Almuqrin, M. Elsafi, Impact of WO3-nanoparticles on silicone rubber for radiation protection efficiency, Materials 15 (2022)

5706, https://doi.org/10.3390/ma15165706.
[28] M.I. Abbas, A.M. El-Khatib, M.F. Dib, H.E. Mustafa, M.I. Sayyed, M. Elsafi, The influence of Bi2O3 nanoparticle content on the γ-ray interaction parameters of silicon rubber, Polymers 14 (2022) 1048, https://doi.org/10.3390/polym14051048.
[29] M.I. Sayyed, H. Al-Ghamdi, A.H. Almuqrin, S. Yasmin, M. Elsafi, A study on the gamma radiation protection effectiveness of nano/micro-MgO-reinforced novel silicon rubber for medical applications, Polymers 14 (2022) 2867, https://doi.org/10.3390/polym14142867.
[30] Y. Al-Hadeethi, M.I. Sayyed, A.Z. Barasheed, M. Ahmed, M. Elsafi, Preparation and radiation attenuation properties of ceramic ball clay enhanced with micro and nano ZnO particles, J. Mater. Res. Technol. 17 (2022) 223–233, https://doi.org/10.1016/j.jmrt.2021.12.109.
[31] M.I. Sayyed, M.F. Alrashedi, A.H. Almuqrin, M. Elsafi, Recycling and optimizing waste lab glass with Bi2O3 nanoparticles to use as a transparent shield for photons, J. Mater. Res. Technol. 17 (2022) 2073–2083, https://doi.org/10.1016/j.jmrt.2022.01.113.
[32] A.N. D'Souza, M.I. Sayyed, N. Karunakara, H. Al-Ghamdi, A.H. Almuqrin, M. Elsafi, M.U. Khandaker, S.D. Kamath, TeO2–SiO2–B2O3 glasses doped with CeO2 for gamma radiation shielding and dosimetry application, Radiat. Phys. Chem. 200 (2022), 110233, https://doi.org/10.1016/j.radphyschem.2022.110233.
[33] E. Şakar, Ö.F. Özpolat, B. Alım, M.I. Sayyed, M. Kurudirek, Phy-X/PSD: development of a user friendly online software for calculation of parameters relevant to radiation shielding and dosimetry, Radiat. Phys. Chem. 166 (2020), https://doi.org/10.1016/j.radphyschem.2019.108496.
[34] E. Hannachi, M.I. Sayyed, Y. Slimani, M.A. Almessiere, A. Baykal, M. Elsafi, Synthesis, characterization, and performance assessment of new composite ceramics towards radiation shielding applications, J. Alloys Compd. 899 (2022), 163173, https://doi.org/10.1016/j.jallcom.2021.163173.
[35] Y. Al-Hadeethi, M.I. Sayyed, A.Z. Barasheed, M. Ahmed, M. Elsafi, Fabrication of lead free borate glasses modified by bismuth oxide for gamma ray protection applications, Materials 15 (2022) 789, https://doi.org/10.3390/ma15030789.
[36] E. Hannachi, M.I. Sayyed, Y. Slimani, M. Elsafi, Experimental investigation on the physical properties and radiation shielding efficiency of YBa2Cu3Oy/M@M3O4 (M= Co, Mn) ceramic composites, J. Alloys Compd. 904 (2022), 164056, https://doi.org/10.1016/j.jallcom.2022.164056.
[37] K.A. Naseer, K. Marimuthu, K.A. Mahmoud, M.I. Sayyed, Impact of Bi2O3 modifier concentration on barium–zincborate glasses: physical, structural, elastic, and radiation-shielding properties, European Phys. J. Plus 136 (2021) 116, https://doi.org/10.1140/epjp/s13360-020-01056-6.
[38] Q. Chen, K.A. Naseer, K. Marimuthu, P.S. Kumar, B. Miao, K.A. Mahmoud, M.I. Sayyed, Influence of modifier oxide on the structural and radiation shielding features of Sm3+-doped calcium telluro-fluoroborate glass systems, J. Australian Ceramic Soc. 57 (2021) 275–286, https://doi.org/10.1007/s41779-020-00531-8.
[39] N.K. Libeesh, K.A. Naseer, K.A. Mahmoud, M.I. Sayyed, S. Arivazhagan, M.S. Alqahtani, E.S. Yousef, M.U. Khandaker, Applicability of the multispectral remote sensing on determining the natural rock complexes distribution and their evaluability on the radiation protection applications, Radiat. Phys. Chem. 193 (2022), 110004, https://doi.org/10.1016/j.radphyschem.2022.110004.
[40] S. Arivazhagan, K.A. Naseer, K.A. Mahmoud, K.V. Arun Kumar, N.K. Libeesh, M.I. Sayyed, M.S. Alqahtani, E.S. Yousef, M.U. Khandaker, Gamma-ray protection capacity evaluation and satellite data based mapping for the limestone, charnockite, and gneiss rocks in the Sirugudi taluk of the Dindigul district, India, Radiat. Phys. Chem. 196 (2022), 110108, https://doi.org/10.1016/j.radphyschem.2022.110108.